

THE EFFECTS OF HEAT BALANCE ON THE VOID FORMATION WITHIN MARAGE 300 PROCESSED BY SELECTIVE LASER MELTING

T. Burkert*, A. Fischer**

*BMW Group, Rapid Technologies Center, Knorrstraße 147, 80788 Munich, Germany

** University Duisburg-Essen, Material Science and Engineering, Lotharstraße 1, 47057 Duisburg, Germany

Abstract

This contribution shows the results of a study that was conducted on the effects of varying selective laser melting (SLM) process parameters on the formation of microstructural voids within a maraging steel (type: Marage 300, 1.2709, AMS6514). Due to the large number of process variables the most influential parameters were identified first. These were energy input resulting from scanning speed, hatch distance, and layer thickness as well as the preheating of the platform. On the basis of the variation of these parameters the most abundant voids were identified and characterized by metallographic investigations. Subsequently tensile tests derived information about the influence of such voids on the mechanical properties. Based on these analyses the reasons for the generation of such voids are discussed followed by strategies in order to prevent them. This allowed for the well-aimed optimization of the processing parameters resulting in a nearly void-free SLM processing of such maraging steel parts.

Keywords: Selective Laser Melting, Direct Metal Laser Sintering, Lasercusing, Maraging Steel, heat balance, mechanical properties, Energy input, preheat temperature, void, defect

1. Introduction

Under the term additive manufacturing a variety of different technologies for generating parts from 3D-CAD-Data is combined. One of the most famous technologies of these is the selective laser melting process (SLM) which provides the layer wise production of high functional parts for testing applications and small series production (e.g. medicine and dental) out of metals. [GIB10], [HUA13], [KRU04], [ZAE11], [ZHA14]

A special feature of the SLM-process and the additive manufacturing at itself is the high degree of geometrical freedom delivered and the opportunity of the process to produce parts without any kind of tools. These two factors, on the one hand the geometrical freedom, which can be used to apply a high grade of individualization in terms of for example personalization or weight reduction and on the other hand the opportunity to conduct production in flexible lot sizes without the need of tools. Cause of these advantages additive manufacturing nowadays is used in both prototyping and small-series production. [CAM12], [GRZ11], [PET11]

In the development of the SLM process there have been several material research topics (e.g. for aluminium, stainless steel or titanium) targeting an increase of the parts density and the void prevention. The Reason is that these factors affect the mechanical properties, such as strength and hardness, positively. It has been shown that parts processed via SLM can attain comparable

mechanical properties to corresponding conventionally processed ones. [BUC11], [KON11], [KRU10], [ZHA14]

The concrete influence of voids, respectively defects has been investigated in particular for the material Ti-6Al-4V. It has been found that the defects has a significant influence on both the static mechanical properties and the high cycle fatigue. [GRE13], [WCY14]

The influence of various process parameters, such as energy input, on the porosity and meltpool appearance has been shown for both SLM and EBM process in comparison. It is stated that the energy input has a significant influence on the defect generation. For marginal parameters of too low and too high energy input the results are spattered defects on the lower side and round defects on the higher side. [GON13], [GON14], [STO14]

In many cases the use of the geometrical freedom provided is limited due to material effects, such as high residual stresses and cracking, which result from high temperature gradients while processing the material in selective laser melting. [CAM12], [GRZ11], [FUL14]

Resulting from this there is a variety of materials (e.g. aluminium) hard to process without generating defects, such as pores and cracks, when not using a suitable preheating. Other strategies to obtain the high temperature gradients are to use scanning strategies different from the generally used stripe scanning. [BUC11], [KRU14]

Additionally there were researches done, which have shown, that the preheating temperature has a significant impact on the resulting mechanical properties and the microstructure. As already stated above an additionally high impact on the mechanical properties is made by the scanning strategies, which result in different energy input levels and so different temperature gradients while processing. [BUC11]

2. Objective

Due to the lack of knowledge about the exact relationship between process parameters and the appearance of voids within the selective laser melting process it is basically difficult to determine which type of voids tolerable in terms of given requirements. The target of this study in this context is to find correlations of the process parameters energy input and preheat temperature, which are the main parameters defining the in-process heat balance, on the one hand and the resulting void appearance on the other hand for the given material Marage 300 (1.2709). Based on the findings the study furthermore should show the influence of the identified voids on the static mechanical properties and the resulting fracture surfaces.

3. Experimental approach and methods

3.1 Material

For the purpose of this study the material processed by SLM is Marage 300 (1.2709/AMS-6514). Before processing an initial characterization of the powder has been done and shown below in Detail. The concrete investigations, which have been done are:

- Chemical analysis based on induced coupled plasma optical emission spectrometry (ICP-OES) (cp. figure 1)
- Fraction characterization based on Camsizer XT (Co. Retsch) using dynamic image analysis (cp. figure 2)
- Image acquisition based on scanning electron microscopy using SEM type Supra (Co. Zeiss) (cp. figure 3)

Chemical analysis Marage 300		
Alloying element	target [%]	actual [%]
Fe	base	base
C	< 0,03	0,01
Si	< 0,1	0,07
Mn	< 0,15	0,03
Ni	17,0 - 19,0	18,4
Mo	4,5 - 5,2	5,1
Ti	0,8 - 1,2	1,03
Co	8,5 - 10,0	9,6
Cr	< 0,25	0,16

Figure 1: Chemical analysis Marage 300 (ICP-OES)

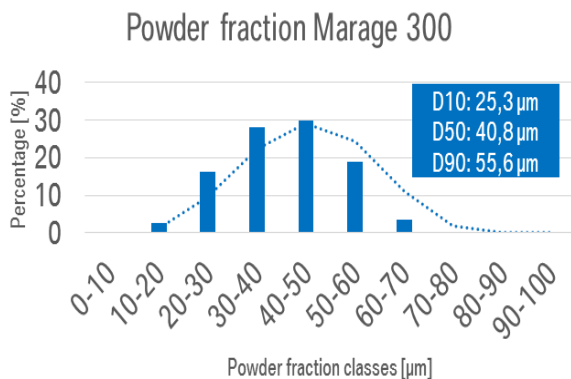


Figure 2: Fraction characterization Marage 300 (Camsizer XT)

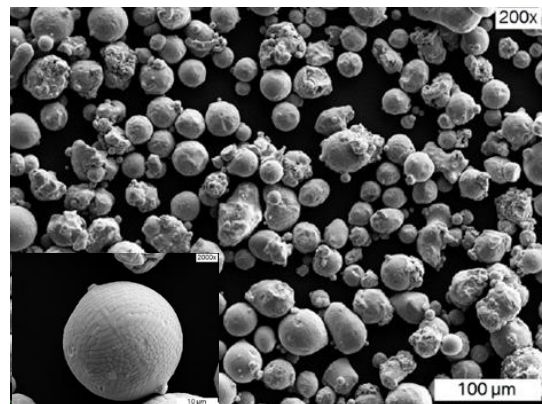


Figure 3: SEM-image of Marage 300 powder

Based on the initial investigations shown in Figures 1-3 the powder used in the studies is completely characterized in terms of chemical composition, fraction and shape. It fulfills on the one hand the chemical composition targets coming from AMS6514 (cp. figure 1) and shows the

other hand a powder fraction of D10: 25,3 μm, D50: 40,8 μm and D90: 55,6 μm (cp. figure 2). Furthermore the powder shape is mostly spherical (cp. figure 3) with few adhesions.

3.2 Machine and parameters

The machine used to process the specimen for the study is a Realizer SLM 100 with a 200 W Fiberlaser and Gaussian laser profile (general setup shown in Figure 4). Basically there are process parameters which has been fixed within the study (cp. figure 5) to gain the clear correlation between the variable parameters (cp. figure 6) stated.

The variable parameters within the experiments are:

- preheat temperature, which is varied in 50 °C-steps between 25 °C and 300 °C
- energy input, which is varied in 10 J/mm³-steps between 50 J/mm³ and 140 J/mm³

The variation of the energy input, since it is no direct process parameter, is conducted by varying the scanning speed between 300 mm/s and 900 mm/s and using the following equation (1) to calculate the resulting energy input:

$$E_V = \frac{P_L}{v_S * \Delta y_S * D_S} \quad (1)$$

Machine	
Realizer SLM 100	
Building volume [mm ³]	125x125x100
Max. laser power [W]	200
Laser type [-]	Fiberlaser
Laser spot diameter [mm]	0,02
Laser profile [-]	Gaussian

Figure 4: General machine setup

Fixed Parameters		Variable Parameters	
Laser power P _L [W]	190	Preheat temperature [°C]	25 - 300
Hatch distance Δy _S [mm]	0,08	Scanning Speed v _S [mm/s]	300 - 900
Layer thickness D _S [mm]	0,05	Energy input E _V [J/mm ³]	50-140
Building direction [-]	90° ref. to BP		
Scanning strategy [-]	alternating meander		

Figure 6: variable parameters

Figure 5: Fixed parameters

3.3 Analysis methods

The specimen, which were used for the initial experiments are cubes of 10x10x10 mm. (cp. figure 7). In order to determine and correlate voids in microstructure the specimen produced by parameter variation the appearing voids has been identified by doing metallographic studies using light microscopy (cp. Figure 8).

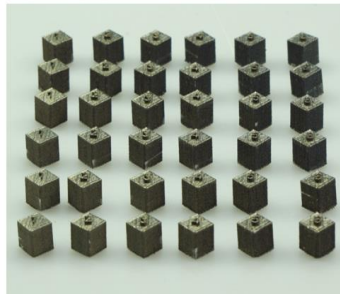


Figure 7: Overview specimen for initial study

Afterwards tensile testing has been done to correlate the appearing voids with their influence on the mechanical properties. The tensile testing has been done with in each case 5 specimen according to DIN 50125 Form A with the parameters 4x20 (cp. Figure 9) based on DIN ISO 6892-1 (cp. figure 10). Finally the tested tensile specimen were further investigated in scanning electron microscope (cp. figure 11) to identify the microstructural behavior and influence of the occurring voids while applying static load.



Figure 8: Light microscope (Leica DM4000 M LED)

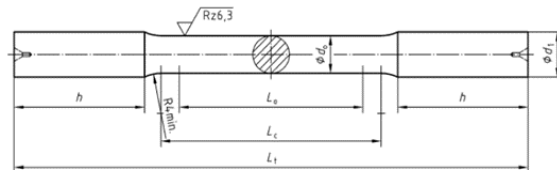


Figure 9: Scheme of tensile specimen (acc. to DIN 50125)



Figure 10: Tensile testing machine (Zwick Proline Z020)



Figure 11: Scanning electron microscope (Zeiss Supra)

4. Results and Discussion

For the beginning of the study the variation of both preheat temperature and energy input is applied to identify the appearing void types and choose the parameter for the correlation via tensile testing. The results of the initial experiment can be seen in figure 12. The next step has been the processing and tensile testing of specimen using the parameters identified in the initial experiment. The last step has been to investigate the fracture surface in both light- and electron scanning microscopy to determine the influence of the appearing voids.

4.1 Microscopic evaluation of initial study

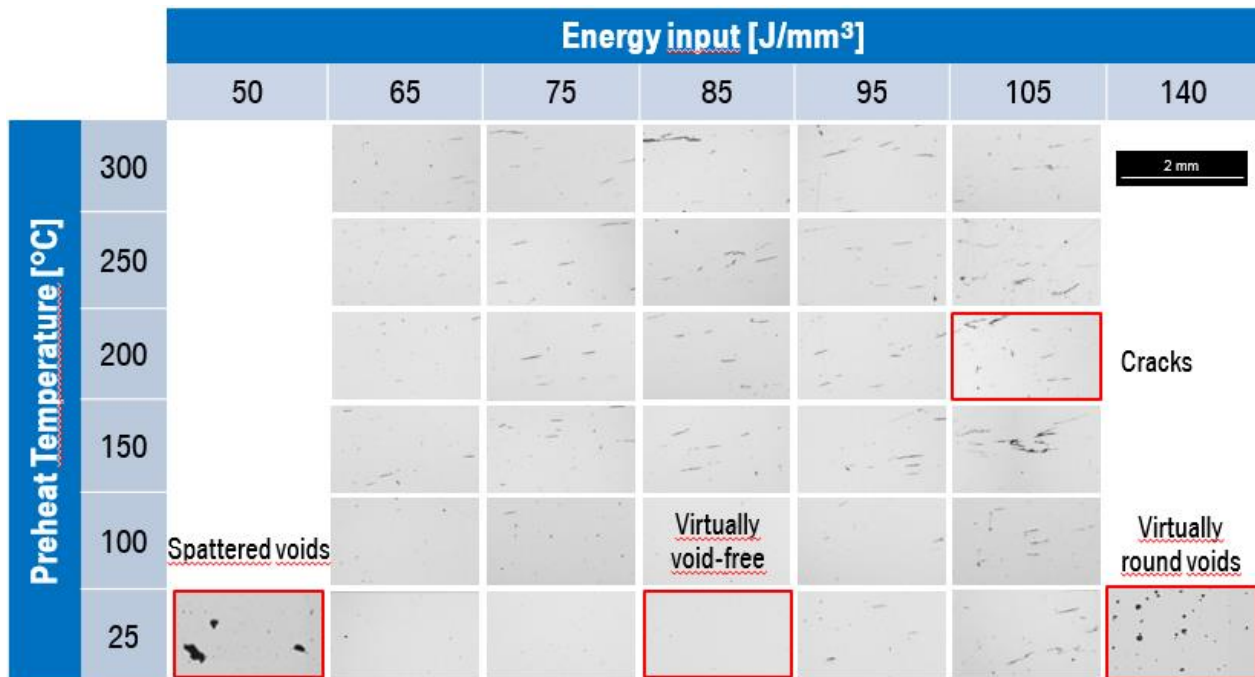


Figure 12: Overview of the initial parameter study

Regarding the results from the initial experiment (cp. figure 12) 4 different types of voids, which appear in different process windows, can be found. Basically they can be described by their shape the following:

- **Spattered voids** appear at a comparatively low energy input (50 J/mm³) and preheat temperature of 25 °C
- **Virtually round voids** appear at a comparatively high energy input (140 J/mm³) and preheat temperature of 25 °C
- **Cracks** appear in very wide area of both energy input and preheat temperature. Regarding the preheat temperature the area of appearance is 100 25 °C (for energy input of 95 J/mm³ to 105J/mm³) and 300 °C for 65 J/mm³ to 105 J/mm³
- The **virtually void-free** area appears between 65 J/mm³ and 85 J/mm³ at a preheat temperature of 25 °C

The parameters, which has been used for the further specimen building has been marked in red in figure 12.

4.2 Tensile testing

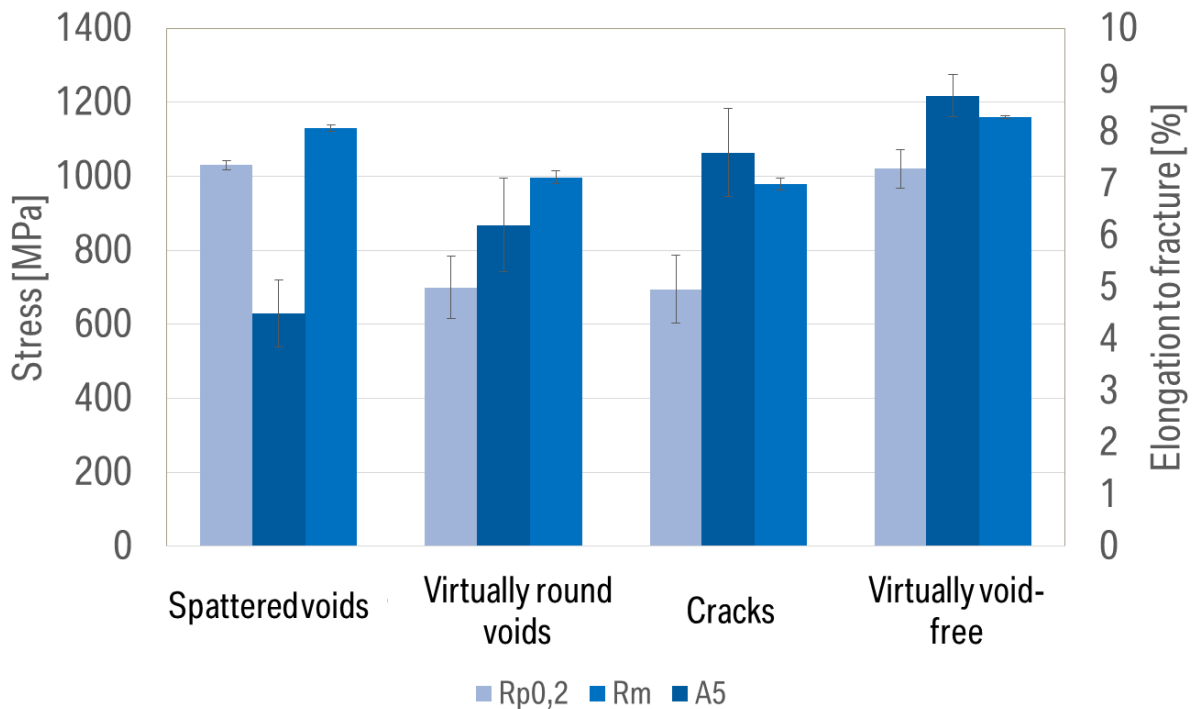


Figure 13: Results of tensile testing

In figure 13 the overview about the tensile testing of the specimen with the parameters chosen from the initial experiment is shown. It can be seen that there is a strongly variation of the different mechanical properties due to the voids appearing in the specimen.

In detail it can be stated that the spattered voids has the biggest influence on the elongation to fraction, but in comparison to that the influence on the resulting strengths is very low. The strength level of the specimen with spattered voids is the same as it is for the virtually void-free specimen, which gain the highest strength within the study. The specimen with virtually round voids show a significant decrease of both elongation to fracture and strengths. In comparison to the spattered voids the influence on the elongation to fracture is not as big, but the strong influence on the strength leads together with the specimen containing cracks to the lowest strength in the study. The specimen containing cracks as well as the specimen with the virtually round voids show a significant decrease of strength but only a small decrease of elongation to fracture compared to the virtually void-free specimen.

The next step is to correlate the results from tensile testing with macro- and microfractographical investigations done by light- and electron scanning microscopy.

4.3 Microscopical & fractographical evaluation

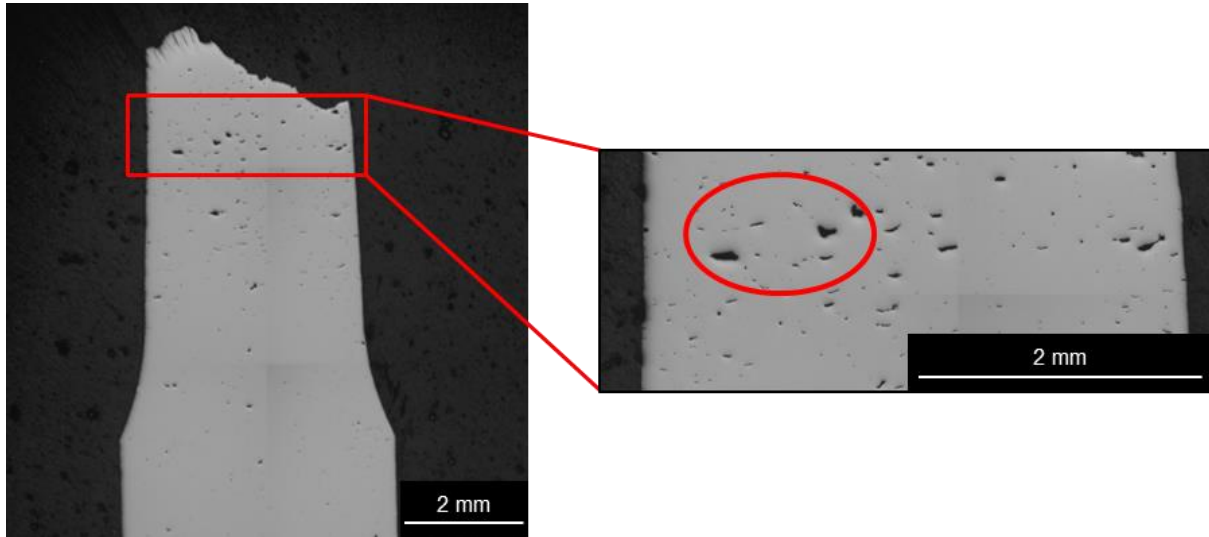


Figure 14: Microscopical image (Overview:left/Detail: right) of tensile specimen with parameter "spattered voids"

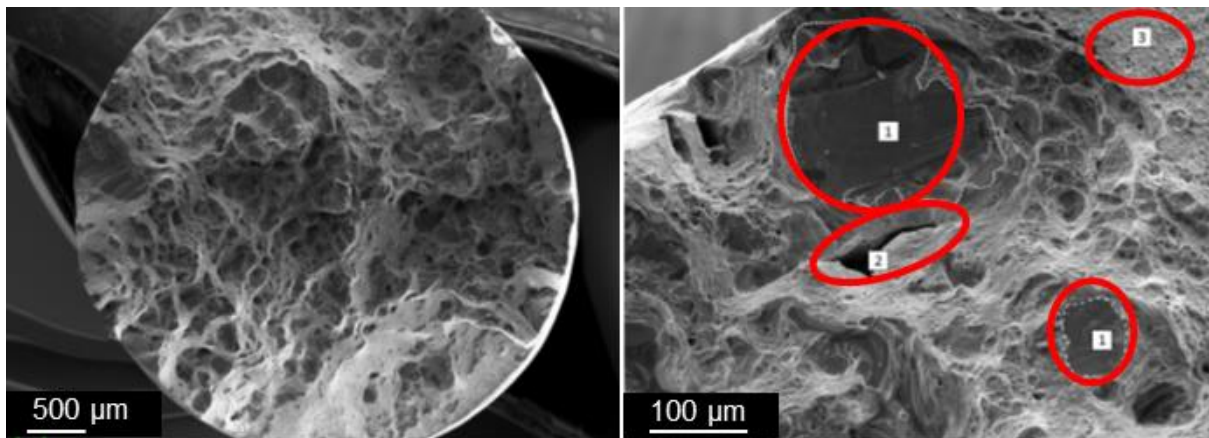


Figure 15: SEM-image (Overview:left/Detail: right) of tensile specimen with parameter "spattered voids"

In Figure 14 the longitudinal cut of one of the tensile specimens with spattered voids is shown as an overview (left) and in detail (right). It can be seen that the specimen has a fracture surface which is diagonal towards the axial orientation of the fracture. The specimen has nearly no deformation, but a high amount of spattered voids within, which are relatively homogeneous distributed over the whole specimen. The topography of the fracture surface is flat.

Figure 15 shows the fracture surface investigated by electron scanning microscopy. On the left side an overview is given and shows a terraced and jagged fracture surface with many relatively big spattered voids. In the detail image on the right side the different appearing microfractographical characteristics. Marked with red circle and number 1 there is are free areas, which means an area which possibly has not been melted with the layers above, in different sizes. Area 2 shows some kind of a crack which goes parallel to the fracture surface. Area 3 shows dimples, guides to ductile behavior of the material in this area.

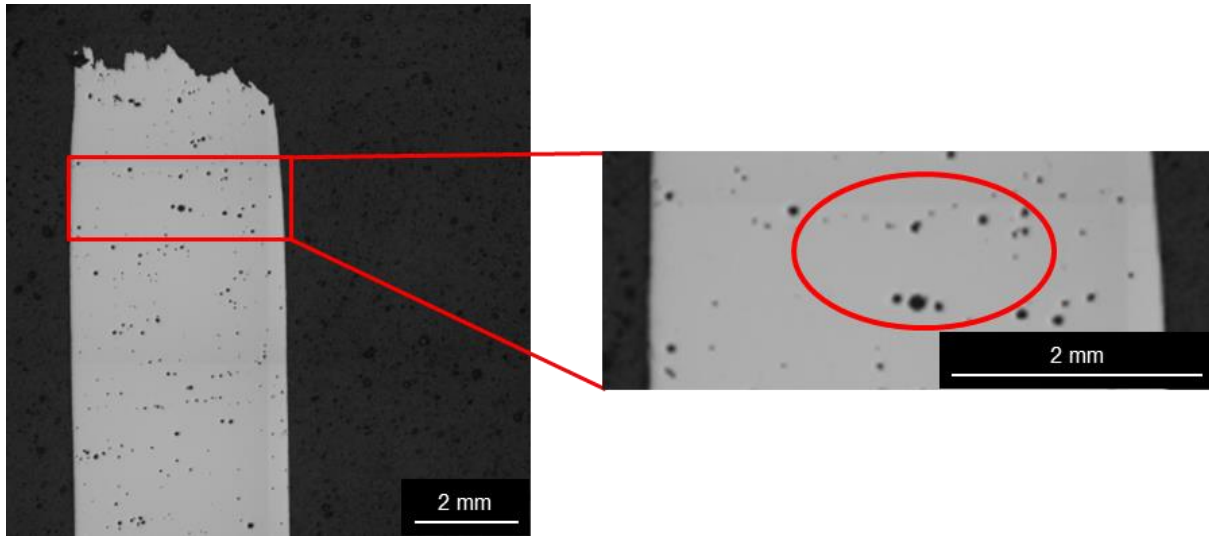


Figure 16: Microscopical image (Overview:left/Detail: right) of tensile specimen with parameter "virtually round voids"

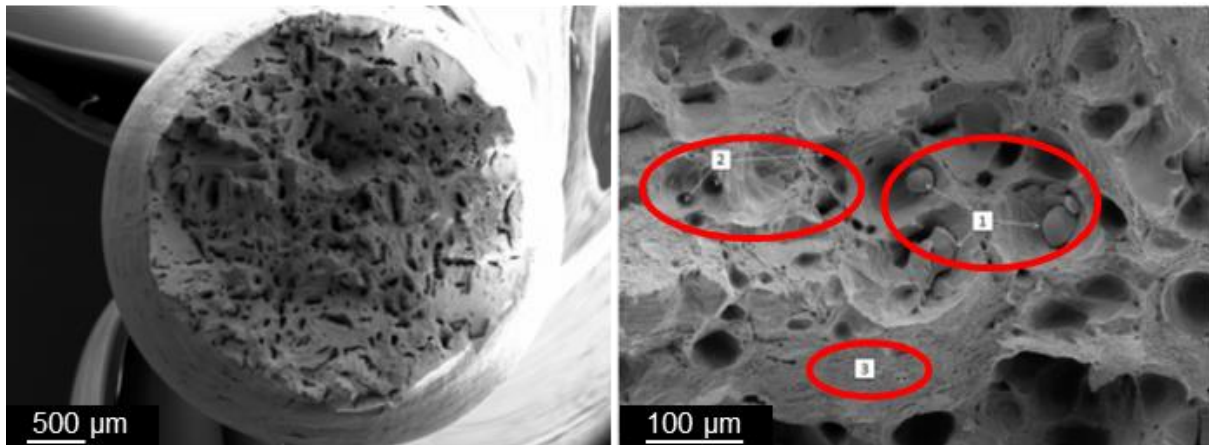


Figure 17: SEM-image (Overview:left/Detail: right) of tensile specimen with parameter "virtually round voids"

In Figure 16 the longitudinal cut of one of the tensile specimens with virtually round voids is shown as an overview (left) and in detail (right). It can be seen that the specimen has a relatively flat fracture surface and is fractured perpendicular to its axial orientation. The topography of the fracture surface is jagged and the specimen has nearly little deformation, but contains a high amount of virtually round voids which are homogeneous distributed over the specimen.

Figure 17 shows the fracture surface investigated by electron scanning microscopy. On the left side an overview is given and shows as already stated a relatively jagged fracture surface containing very many virtually round voids and few linear voids. In the detail image on the right side the different appearing microfractographical characteristics. Marked with red circle in area 1 there are unmolten powder particles showing up. Area 2 shows different sizes of virtually round voids within the fracture surface. Area 3 shows comparable to the specimen with spattered voids an area containing dimples.

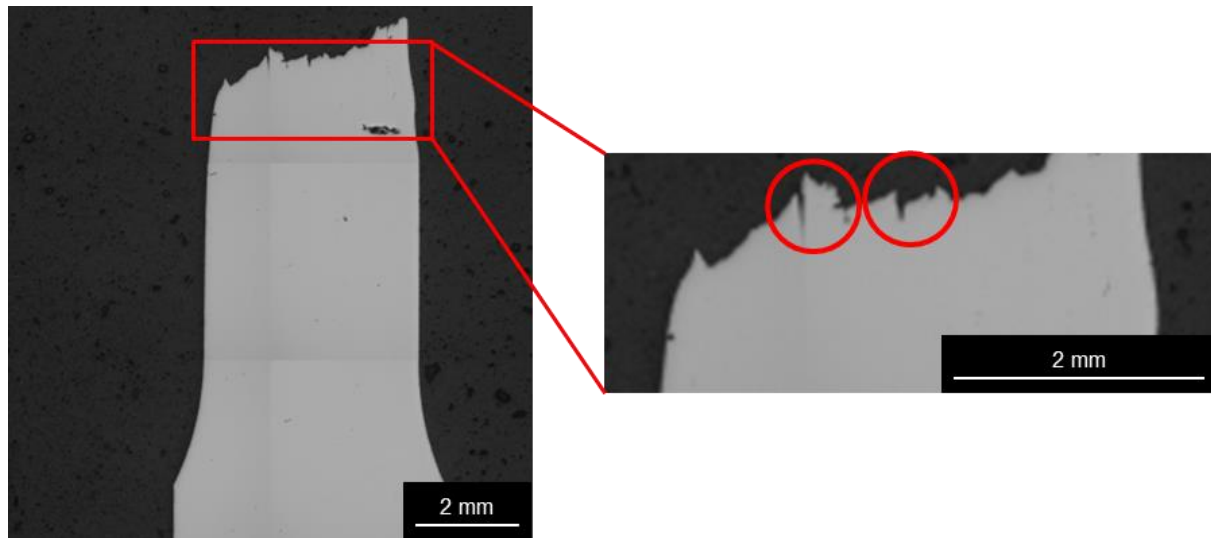


Figure 18: Microscopical image (Overview:left/Detail: right) of tensile specimen with parameter "Cracks"

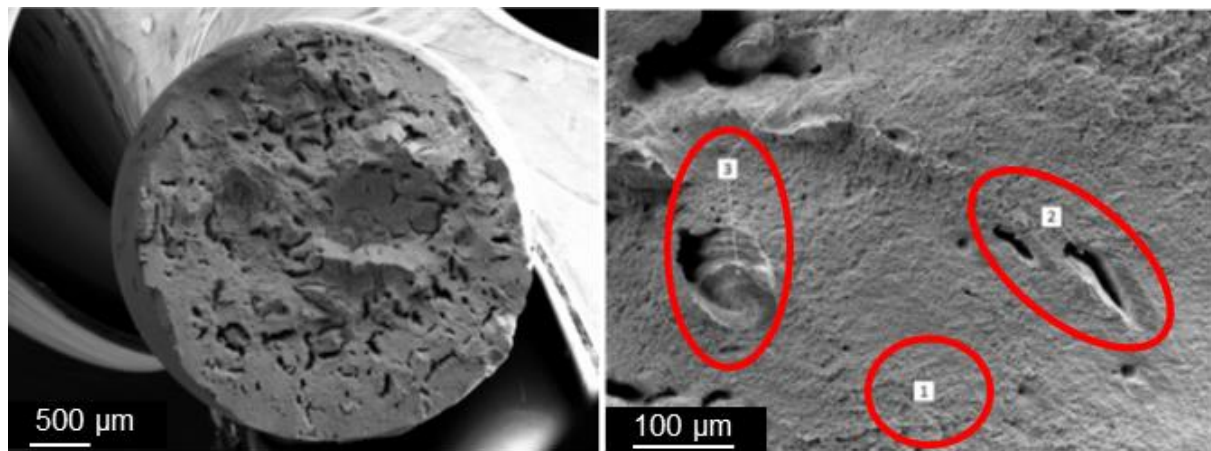


Figure 19: SEM-image (Overview:left/Detail: right) of tensile specimen with parameter "Cracks"

In Figure 18 the longitudinal cut of one of the tensile specimens with cracks is shown as an overview (left) and in detail (right). It can be seen that the specimen is fractured perpendicular to the axial orientation of the fracture and the deformation is considerable compared to the “spattered void” and “virtually round void” specimen. The topography of the fracture surface is relatively flat with little areas which are kind of jagged. On the right image it can be seen that there are cracks within the fracture surface seem to run perpendicular to the fracture surface. The remaining area of the specimen is nearly void free, but for a big spattered void at around 2 mm below the fracture surface.

Figure 19 shows the fracture surface investigated by electron scanning microscopy. On the left an overview is given and shows a relatively flat and only little jagged fracture surface with areas containing many linear voids and other areas being nearly void free. In the detail image on the right side the different appearing microfractographical characteristics. In area 1 very small dimples can be seen, which means ductile areas of the material. Area 2 shows some kind of a secondary cracking which goes parallel to the fracture surface. Area 3 shows a free surface, which is possible not melted to the upper layer and additionally an enclosed cavity.

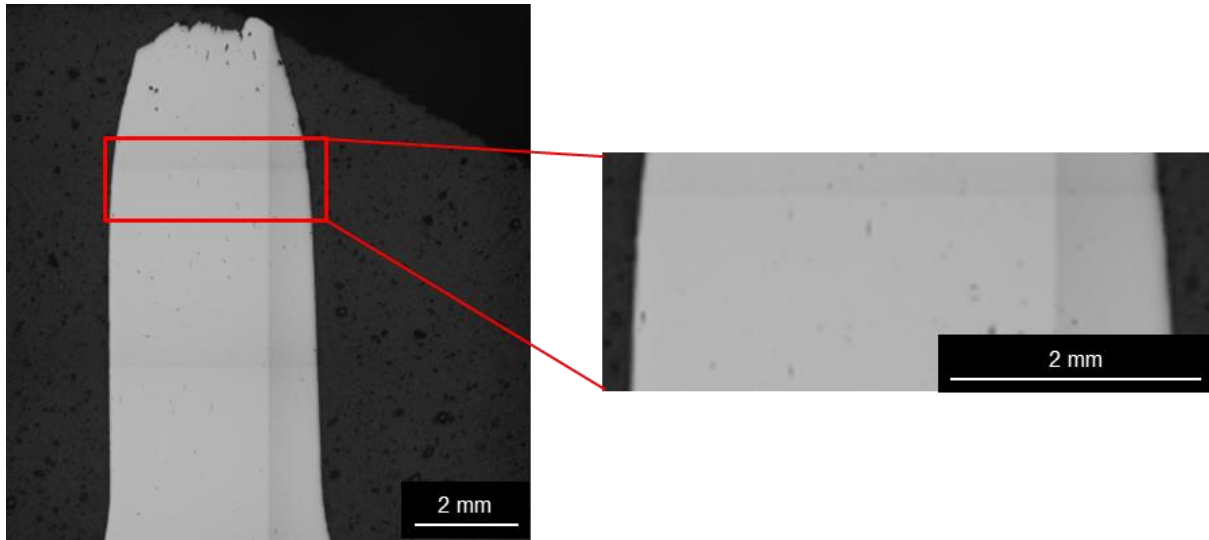


Figure 20: Microscopical image (Overview: left/Detail: right) of tensile specimen with parameter "virtually void-free"

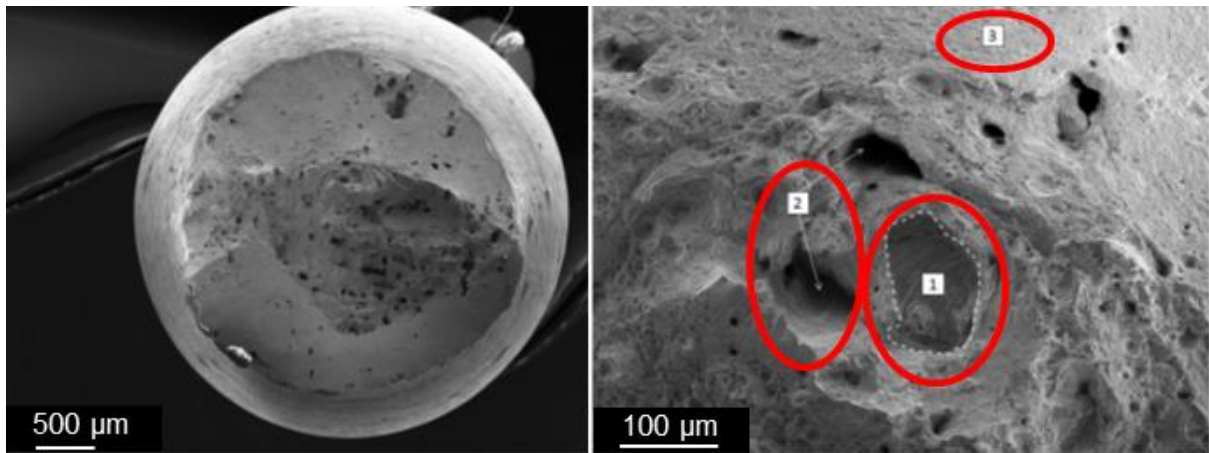


Figure 21: SEM-image (Overview: left/Detail: right) of tensile specimen with parameter "virtually void-free"

In Figure 20 the longitudinal cut of one of the tensile specimens which has been nearly void free is shown as an overview (left) and in detail (right). It can be seen that the specimen is fractured perpendicular to the axial orientation of the specimen. Additionally it can be stated that the specimen has a relatively flat and only little jagged fracture surface with considerable deformation and a few spattered voids straight below the fracture surface. The rest of the specimen, as it can be seen on the right side is nearly void free.

Figure 21 shows the fracture surface investigated by electron scanning microscopy. On the left side an overview is given and shows a flat and only little jagged fracture surface with in comparison to the prior specimen few mainly round and few spattered voids, which are concentrated in the middle of the fracture surface. The considerable deformation of the specimen results in a decrease of the investigated fracture surface. In the detail image on the right side the different appearing microfractographical characteristics are highlighted. Area 1 is showing free surfaces, which possibly guide to a layer which is unmolded with the above layer. Area 2 shows the already stated round to spattered voids appearing and number 3 an area of small dimples.

Comparing the 4 different parameter setups resulting from the void identification of the initial experiments the results show that the exact processing parameters have a huge influence on the resulting density and appearing voids. On the other hand the further results from tensile testing and metallo- and fractography show that the different void types have a significant influence on both the mechanical properties and the appearance of the fracture surface after tensile testing.

In terms of mechanical properties spattered voids have the biggest influence on the elongation on fracture, which means a decrease of about 50% in comparison to the virtually void-free specimen. Virtually round voids and cracks in contrast have the biggest influence on the strengths. The decrease in strength is about 13% in case of tensile strength and 34% regarding the comparable yield strength of the virtually void-free specimen.

Regarding the fracture surfaces the results show that there are voids in any of the specimen but that their appearance in terms of size and number varies from parameter setup to parameter setup. The spattered voids parameter setup for example is resulting in free surfaces, corresponding with unmolded neighbored layer, which are showing up in smaller fashion at the fracture surface of the virtually void-free parameter setup as well. In contrast to that the virtually round voids parameter shows mainly unmolded powder particles and many round voids in the fracture surface. The cracks parameter setup in comparison shows cracks running parallel and perpendicular to the fracture surface as characteristics. All of the specimen has in common that there is always an area of dimples, which can possibly guide to ductile fracture behavior.

5. Conclusions

The characterization of the different kinds of the apparent voids for the maraging steel marage 300 subject to the energy input and the preheat temperature has been done. Therefore exact process windows for each void type has been identified and the influence of energy input and preheat temperature on the appearance has been shown. Regarding to that the identification and characterization of the apparent voids could be done.

The correlation of the apparent voids and resulting mechanical properties from tensile testing has been done on parameter setup layer. Furthermore the influence of the apparent voids in perpendicular building direction on the mechanical properties has been shown.

Metallography and fractography has shown the different appearance of the voids in both longitudinal cut and fracture surface. The void types which has been identified through the initial experiment and following metallography has been found and confirmed in the metallo- and fractography of the tensile specimen. The parameter setup “virtually void-free” shows voids in the fracture surface, which guides to the conclusion that there is a further optimization and investigation necessary to determine the optimal processing parameters. Nevertheless the mechanical properties show higher elongation and strength as well as the cut and fracture surfaces show less to no voids in comparison to the specimen of the other parameter setups.

For further research the main areas of interest has been identified and should be:

- Further investigations to identify the reasons for appearance of the different voids
- Further correlation of the appearing voids with other process parameters (e.g. powder quality, laser profile, ...)

- Transfer and validation of the results:
 - in dynamic and cyclic mechanical testing of specimen
 - in prototype parts from automotive applications

6. References

- [BUC11] Buchbinder D, et al. Untersuchung zur Reduzierung des Verzugs durch Vorwärmung bei der Herstellung von Aluminiumbauteilen mittels SLM. *RTEjournal - Forum für Rapid Technologie*, 8(1). 2011.
- [CAM12] Campbell I, et al. Additive manufacturing: rapid prototyping comes of age. *Rapid prototyping journal*, Vol. 18 No. 4, pp. 255–258. 2012.
- [FUL14] Fulcher B A, et al. Comparison of AlSi10Mg and Al 6061 processed through DMLS. *Solid Freeform Fabrication Symposium 2014*, Austin. 2014.
- [GIB10] Gibson I, et al. *Additive manufacturing technologies: Rapid prototyping to direct digital manufacturing*. Springer, New York, NY. 2010.
- [GON13] Gong H, et al. The Effects of Processing Parameters on the Defect Regularity in Ti-6Al-4V Parts fabricated by Selective Laser Melting and Electron Beam Melting. *Proceedings: Solid Freeform Fabrication Symposium 2013*, Austin. 2013.
- [GON14] Gong H, et al. Analysis of defect generation in Ti-6Al-4V parts made using powder bed fusion additive manufacturing process. *Additive Manufacturing Vol. 1-4*, pp. 87-98. 2014.
- [GRE13] Greitemeier D, et al. Additive Layer Manufacturing of Ti-6Al-4V and ScalmalloyRP®: Fatigue and Fracture. *27th ICCAF Symposium*, Jerusalem. 2013.
- [GRZ11] Grzesiak A, et al. The Bionic Handling Assistant: a success story of additive manufacturing. *Assembly Automation*, Vol. 31 No. 4, pp. 329–333. 2011.
- [HUA13] Huang Y, et al. *Frontiers of Additive Manufacturing Research and Education: An NSF Additive Manufacturing Workshop Report*. 2013.
- [KON11] Kong C-J, et al. High Density Ti6Al4V via SLM Processing: Microstructure and Mechanical Properties. *Proceedings: Solid Freeform Fabrication Symposium 2011*, Austin. 2011.
- [KRU04] Kruth J-P, et al. Selective laser melting of iron-based powder. *Journal of Materials Processing Technology*, 149(1-3), 616-622. 2004.
- [KRU10] Kruth J-P, et al. Part and material properties in selective laser melting of metals. *Proceedings of the 16th International Symposium on Electromachining*, Shanghai. 2010
- [STO14] Stoffregen H A, et al. Fatigue Analysis in Selective Laser Melting: Review and Investigation of Thin-Walled Actuator Housings. *Proceedings: Solid Freeform Fabrication Symposium 2014*, Austin. 2014.
- [WYC14] Wycisk E, et al. Effects of Defects in Laser Additive Manufactured Ti-6Al-4V on Fatigue Properties. *Physics Procedia Vol. 56*, pp. 371-378. 2014.
- [ZAE11] Zaeh M-F, et al. Investigations on heat regulation of additive manufacturing processes for metal structures. *CIRP Annals - Manufacturing Technology*, In Press, Corrected Proof. 2011.
- [ZHA14] Zhai Y, et al. Additive Manufacturing: Making Imagination the Major Limitation. *JOM*, Vol. 66 No. 5, pp. 808–816. 2014.